PGH_2 Degradation Pathway Catalyzed by GSH−Heme Complex Bound Microsomal Prostaglandin E_2 Synthase Type 2: The First Example of a Dual-Function Enzyme[†,‡]

Taro Yamada and Fusao Takusagawa*

Department of Molecular Biosciences, University of Kansas, 1200 Sunnyside Avenue, Lawrence, Kansas 66045-7534

Received March 29, 2007; Revised Manuscript Received May 16, 2007

ABSTRACT: Prostaglandin E_2 synthase (PGES) catalyzes the isomerization of PGH_2 to PGE_2. PGES type 2 (mPGES-2) is a membrane-associated enzyme, whose N-terminal section is apparently inserted into the lipid bilayer. Both intact and N-terminal truncated enzymes have been isolated and have similar catalytic activity. The recombinant N-terminal truncated enzyme purified from *Escherichia coli* HB101 grown in LB medium containing δ-aminolevulinate and $Fe(NO_3)_3$ has a red color, while the same enzyme purified from the same *E. coli* grown in minimal medium has no color. The red-colored enzyme has been characterized by mass, fluorescence, and EPR spectroscopies and X-ray crystallography. The enzyme is found to contain bound glutathione (GSH) and heme. GSH binds to the active site with six H-bonds, while a heme is complexed with bound GSH forming a S−Fe coordination bond with no polar interaction with mPGES-2. There is a large open space between the heme and the protein, where a PGH_2 might be able to bind. The heme dissociation constant is 0.53 μM, indicating that mPGES-2 has relatively strong heme affinity. Indeed, expression of mPGES-2 in *E. coli* stimulates heme biosynthesis. Although mPGES-2 has been reported to be a GSH-independent PGES, the crystal structure and sequence analysis indicate that mPGES-2 is a GSH-binding protein. The GSH−heme complex-bound enzyme (mPGES-2h) catalyzes formation of 12(*S*)-hydroxy-5(*Z*),8(*E*),10(*E*)-heptadecatrienoic acid and malondialdehyde from PGH_2, but not formation of PGE_2. The following kinetic parameters at 37 °C were determined: $K_M = 56$ μM, $k_{cat} = 63$ s^{-1}, and $k_{cat}/K_M = 1.1 \times 10^6$ M^{-1} s^{-1}. They suggest that mPGES-2h has significant catalytic activity for PGH_2 degradation. It is possible that both GSH-heme complex-free and -bound enzymes are present in the same tissues. mPGES-2 in heme-rich liver is most likely to become the form of mPGES-2h and might be involved in degradation reactions similar to that of cytochrome P450. Since mPGES-2 is an isomerase and mPGES-2h is a lyase, mPGES-2 cannot simply be classified into one of six classes set by the International Union of Biochemistry and Molecular Biology.

Prostaglandin E (PGE_2) is widely distributed in various organs and exerts control over various biological activities such as smooth muscle dilation and contraction (*1*), Na^+ excretion (*2*), body temperature (*3*), and the physiological sleep−wake cycle (*4*, *5*). PGE_2 is generated at sites of inflammation in substantial amounts and can mediate many of the pathologic features of inflammation (*6*). PGE_2 is also a potent vasodilator (*7*) and can act synergistically with other mediators and chemotaxins to increase microvascular permeability (*8*). In conjunction with cytokines, PGE_2 is a central mediator of febrile responses (*9*), and intradermal PGE_2 is hyperalgesic in the peripheral nervous system, suggesting that PGE_2 is a powerful fever inducer (*10*). Several nonsteroidal anti-inflammatory drugs such as sulindac sulfide, NS-398, and indomethacin (IMN)[1] inhibit not only COX but also prostaglandin E_2 synthase (PGES) to reduce fever and pain (*11*, *12*).

PGES catalyzes the isomerization of PGH_2 to PGE_2. At least three different types of mammalian PGE_2 synthase have been isolated. A cytosolic enzyme has been purified from the cytosol of human brain and *Ascaridia galli* (*13*−*15*). This cytosolic enzyme is a GSH-dependent enzyme and is called cPGES (*15*). Membrane-associated PGES type 1 (mPGES-1) was enriched from microsomal fractions of bovine and sheep vesicular glands (*16*, *17*) and shown to require GSH. Tanaka et al. (*18*) characterized mPGES-1 in sheep vesicular gland microsomes by use of two monoclonal antibodies and determined the kinetic property and molecular mass. Jakob-

[†] The work has been partially supported by grants from the American Heart Association (045545Z) and the Arthritis Foundation.

[‡] The atomic coordinates and structure factors have been deposited with the Protein Data Bank (entry 2PBJ).

* To whom correspondence should be addressed: Department of Molecular Biosciences, 3004 Haworth Hall, University of Kansas, 1200 Sunnyside Ave., Lawrence, KS 66045-7534. Telephone: (785) 864-4727. Fax: (785) 864-5321. E-mail: xraymain@ku.edu.

[1] Abbreviations: ALA, δ-aminolevulinate; COX, cyclooxygenase; COX-1, COX type 1; COX-2, COX type 2; GSTase, glutathione *S*-transferase; HHT, 12(*S*)-hydroxy-5(*Z*),8(*E*),10(*E*)-heptadecatrienoic acid; hPGDS, hematopoietic prostaglandin D_2 synthase; IMN, indomethacin; MDA, malondialdehyde; mPGES-1, microsomal prostaglandin E_2 synthase type 1; mPGES-2, microsomal prostaglandin E_2 synthase type 2; mPGES-2[GSH−heme + PGH_2], GSH−heme complex- and PGH_2-bound mPGES-2; mPGES-2[GSH−heme], GSH−heme complex-bound mPGES-2; mPGES-2[IMN], IMN-bound mPGES-2; mPGES-2h, GSH−heme complex-bound mPGES-2; PGES, prostaglandin E_2 synthase; TxA_2, thromboxane A_2; TXAS, TxA_2 synthase.

10.1021/bi700605m CCC: $37.00
Published on Web 06/22/2007

sson et al. (*19*, *20*) expressed human mPGES-1 in *Escherichia coli* and have carried out biochemical characterizations, including a low-resolution structure determination by electron diffraction crystallography.

Watanabe et al. (*21*, *22*) reported that PGES activity was widely distributed in the microsomal fractions of rat and sheep organs. The membrane-associated enzyme was purified from the microsomal fraction of bovine heart, and its enzymatic properties were examined (*22*). Although most of the PGES activity in many organs absolutely requires GSH, Watanabe et al. reported that the enzyme activity in heart, spleen, and uterine microsomes did not specifically require GSH for its catalytic activity, as GSH could be replaced by other reducing reagents (*23*). This GSH-independent membrane-associated PGES was different from mPGES-1 reported by Jakobsson et al. (*19*), and it was named mPGES-2. The N-terminal truncated enzyme was found in the microsomal fraction of bovine heart. The N-terminal sequence of the truncated enzyme starts from Glu88 of the protein derived from the human cDNA (*22*). The intact and the N-terminal truncated mPGES-2 had similar catalytic activities. The intact and the N-terminal truncated proteins expressed in *E. coli* have the same enzymatic properties as the enzyme purified from bovine heart microsomes (*23*). We determined the crystal structure of N-terminal truncated mPGES-2 bound to an inhibitor indomethacin (IMN) and proposed a possible catalytic mechanism for formation of PGE_2 from PGH_2 (*24*).

The recombinant N-terminal truncated mPGES-2 purified from the recombinant clone *E. coli* HB101 grown in LB medium had a red color. However, no significant electron density for compounds that produce a red color was found in the crystal structure of mPGES-2[IMN]. We have carried out a characterization of the red-colored mPGES-2 by mass, fluorescence, and EPR spectroscopies and X-ray crystallography. Here we report that the red enzyme contains a GSH−heme complex in the active site, which catalyzes degradation of PGH_2 but not formation of PGE_2.

MATERIALS AND METHODS

Purification of the Red-Colored Enzyme (mPGES-2h). The gene of the human mPGES-2 with N-terminal residues 1−87 truncated was cloned into the pTrc-HisA vector and transformed into *E. coli* HB101 (*23*). The *E. coli* was grown at 37 °C in 1 L of LB medium containing 50 mg of ampicillin, 100 mg of δ-aminolevulinate (ALA), and 100 mg of $Fe(NO_3)_3$. IPTG was added to a final concentration of 1 mM after the sample had been cultured for 1.5 h, and incubation was continued for an additional 15 h. Cells were harvested by centrifugation and suspended in 60 mL of a buffer [50 mM Tris-HCl (pH 7.5) and 0.5 mM EDTA]. Cell lysis was carried out by treatment with egg white lysozyme (1 mg/mL of the suspension at 0 °C for 1 h), followed by freezing and thawing. The mixture was subjected to a brief sonication. The centrifuged supernatant was treated with 300 g/L ammonium sulfate, and the precipitated protein was recovered by centrifugation. Ammonium sulfate, EDTA, and Tris-HCl were removed by dialysis in buffer A [30 mM potassium phosphate (pH 7.2) and 0.2% Tween 20]. The protein was loaded onto a column of DE52 (2.4 cm × 10 cm) equilibrated with buffer A. The enzyme was eluted via a linear gradient between 100 mL each of 30 and 200 mM potassium phosphate (pH 7.2) containing 0.2% Tween 20. Fractions having a red color were pooled, and imidazole was added to a final concentration of 10 mM. The solution was mixed with 8 mL of nickel-chelating resin [Ni-CAM HC Resin (Sigma)] equilibrated with 30 mM potassium phosphate buffer (pH 7.2) containing 10 mM imidazole. After the sample had been stirred for 1 h at 4 °C, the resin was collected by centrifugation and packed into a column (1.0 cm × 5.0 cm). The column was washed with 30 mM potassium phosphate buffer (pH 7.2) containing 10 mM imidazole and 0.01% *n*-dodecyl β-D-maltopyranoside until the absorption at 280 nm of the elute reached that of the washing buffer. The enzyme was eluted via a linear gradient between 50 mL each of 10 and 200 mM imidazole in 30 mM potassium phosphate buffer (pH 7.2) containing 0.01% *n*-dodecyl β-D-maltopyranoside. The red fractions were pooled and concentrated to 20 mg/mL using an Amicon concentrator with a 30 kDa cutoff membrane. The purity of the enzyme was checked by SDS−PAGE.

Purification of the Colorless Enzyme (heme-free mPGES-2). The same recombinant clone *E. coli* HB101 was precultured in LB medium overnight at 37 °C and used to inoculate (5%, v/v) 1 L of minimal medium [1 L contains $(NH_4)_2SO_4$ (1.0 g), KH_2PO_4 (4.5 g), K_2HPO_4 (10.5 g), sodium citrate (0.5 g), 20 L-amino acids (40 mg each), adenine (125 mg), guanosine (125 mg), thymine (125 mg), uracil (125 mg), glucose (5 g), $MgSO_4$ (0.12 g), D-biotin (4 mg), thiamine (4 mg), and ampicillin (100 mg)]. After the sample had been cultured for 8 h, IPTG (100 mg/L) was added to induce mPGES-2 overnight at 37 °C. The colorless enzyme was purified using the same procedures applied for the red-colored enzyme. Because the colorless protein was relatively unstable and aggregated easily, the purification was carried out in the presence of 0.01% *n*-dodecyl β-D-maltopyranoside. The purity of the enzyme was checked by SDS−PAGE.

Purification of the C110S Mutated mPGES-2. The pTrc-HisA vector containing the C110S mutated mPGES-2 gene was transformed into *E. coli* HB101 (*25*). The *E. coli* was grown in the same medium used for the red-colored enzyme. The C110S mutated mPGES-2 was purified with the same procedures described above. The red-colored protein was obtained, and the purity of the protein was checked by SDS−PAGE.

Heme Titration Measurements. Trp fluorescence spectra were recorded at 25 °C using a Cary Eclipse fluorescence spectrophotometer (Varian). The intrinsic fluorescence of the Trp residues of mPGES-2 was measured after addition of 5 μL of 30 μM hematin (heme) in DMSO and 5 μL of 30 μM GSH to 3.0 mL of 1.0 μM colorless enzyme (mPGES-2) in sodium phosphate buffer (pH 7.2). Emission spectra were recorded at an interval of 1 nm between 300 and 450 nm with an excitation wavelength of 280 nm, at a slit width of 4 nm. The titration was repeated 24 times, and 25 fluorescence emission spectra were obtained. Correction for light scattering was not carried out because the corresponding spectra of heme did not exhibit an emission spectrum. Enzyme−heme binding was analyzed from the quenching of the intrinsic Trp fluorescence intensity of the enzyme.

Determination of the Crystal Structure of Red mPGES-2h. The enzyme used in this study is a recombinant protein, N-terminal amino acid residues 1−87 of which were

truncated, and a His tag was attached to residue 88. The red mPGES-2 was crystallized using a sitting-drop vapor diffusion method. The crystallization conditions were as follows: 1.7 M ammonium sulfate, 100 mM sodium acetate/HCl buffer (pH 5.5), and 10 mg/mL enzyme. Red plate crystals were grown in 3 days at 22 °C. A crystal having dimensions of ~0.3 mm × 0.2 mm × 0.1 mm in a drop was scooped out with a nylon loop and was dipped into a cryoprotectant solution containing 25% ethylene glycol, 1.2 M ammonium sulfate, and 100 mM sodium acetate/HCl (pH 5.5) for 30 s before it was frozen in liquid nitrogen. The frozen crystal was transferred onto a Rigaku RAXIS IIc imaging plate X-ray diffractometer with a rotating anode X-ray generator as an X-ray source (Cu Kα radiation operated at 50 kV and 100 mA). The X-ray beam was focused to 0.3 mm by confocal optics (Osmic, Inc.). The diffraction data were measured up to 2.8 Å resolution at −180 °C. The data were processed with DENZO and SCALEPACK (*26*).

The unit cell dimensions and the assigned space group indicated the red crystal is isomorphous to that of mPGES-2[IMN] (*24*), and two dimeric enzymes (four subunits) were in the asymmetric unit. The crystal structure was refined by a standard refinement procedure in the CNS protocol with the noncrystallographic symmetry restraint (*27*). During the later stages of refinement, difference maps ($F_o - F_c$) showed large flat and elongated residual electron density peaks in the region of the active site of each subunit. An anomalous dispersion difference map [$F_o(+) - F_o(-)$] exhibited a very high peak (7σ) in the middle of the flat residual electron density. A heme molecule was fit into the flat residual electron density peak. Since the elongated residual electron density peak exhibited a GSH molecular shape, a GSH molecule was fit in the residual electron density peak. A CNS refinement has confirmed that the red mPGES-2 is mPGES-2 containing a GSH−heme complex in the active site, mPGES-2[GSH−heme]. During the final refinement stage, well-defined residual electron density peaks in difference maps were assigned to water molecules if peaks were able to bind the protein molecules with H-bonds. The four subunits related by a noncrystallographic 222 symmetry were tightly restrained to have the same structure to increase the accuracy of coordinates. The structure was refined with all reflections (no σ cutoff) from 20 to 2.8 Å resolution. The final coordinates and the structure factors have been deposited in the Protein Data Bank (entry 2PBJ).

Catalytic Rate of Formation of HHT and MDA by mPGES-2h. The following stock solutions were prepared: buffer solution [50 mM potassium phosphate buffer (pH 7.2) containing 2.5 mM GSH], the red enzyme (mPGES-2h) solution (0.5 mg/mL in the buffer solution), and PGH_2 (0.1 mg/mL acetone solution from Cayman). Ten microliters of mPGES-2 and x μL of PGH_2 ($x = 2$, 4, 6, or 8) were added to a tube containing $90 - x$ μL of the buffer solution. The enzyme reaction was carried out for 100 s at 4 °C. (Since PGH_2 is relatively unstable and the catalytic reaction is relatively fast, all experiments were carried out at 4 °C.) The reaction was stopped by adding 100 μL of 0.35% trifluoroacetic acid (TFA). The reaction mixture was poured on a pre-equilibrated PrepSep C_{18} 100 mg column (Fisher Scientific); the column was washed with 2 mL of 0.01% TFA and eluted with acetonitrile (300 μL). The collected solution was diluted with 300 μL of 0.01% TFA, 150 μL of which was injected into a HPLC system (Shimazu LC-6A) with a NovaPak C_{18} column (3.9 mm × 150 mm from Waters) and eluted with 48% acetonitrile containing 0.01% TFA as the mobile phase. The flow rate was 0.7 mL/min, and the product was monitored at 232 nm. After each experiment, a blank experiment was carried out under the same conditions except for the absence of mPGES-2 and $100 - x$ μL of buffer solution. The chromatographs of the experimental and blank samples were the same except for the peak at the retention time of ~10.6 min. The integrated peak area was corrected by subtracting the peak area of the blank experiment.

The other blank experiments that include various concentrations of HHT instead of PGH_2 were carried out to confirm the retention time (10.6 min) of HHT and to make a calibration chart for the HHT concentration determination. The HHT concentrations from the various PGH_2 amounts ($x = 2$, 4, 6, or 8) were calculated from the net integrated peak area and the calibration chart. The kinetic parameters (K_M, V_{max}, and k_{cat}) at 4 °C were determined from a double-reciprocal plot ($1/[PGH_2]$ vs $1/v_o$).

Formation of prostanoids from PGH_2 was also examined by the same procedure described above except for the monitoring wavelength (195 nm). The reaction mixtures did not show any significant peaks corresponding to PGE_2, PGD_2, or $PGF_{2\alpha}$.

Cloning and Purification of Hematopoietic PGD_2 Synthase (hPGDS). cDNA of hPGDS was purchased from OriGene and was amplified by PCR. The amplified fragment was digested with *Nde*I/*Hin*dIII and inserted into the *Nde*I/*Hin*dIII site of pET26b(+) (Novagene). The nucleotide sequence of the amplified DNA fragment was verified by the dideoxy chain termination method at the University of Kansas DNA sequencing lab. The resultant plasmid was used to transform *E. coli* BL21. hPGDS was purified as reported previously (*28*).

Physical Methods. Mass spectra were recorded on a VG ZAB high-resolution double-focusing instrument. EPR spectra were collected using a Bruker EMX spectrometer equipped with an ER041XG microwave bridge. Spectra for EPR samples were collected using the following spectrometer settings: microwave power, 5.041 mW; frequency, 9.45 GHz; sweep width, 5000 G; modulation amplitude, 10.02 G; gain, 1.00×10^3; conversion time, 81.920 ms; time constant, 655.36 ms; and resolution, 1024 points. Low-temperature (4 K) spectra were obtained using an Oxford Instruments liquid He quartz cryostat.

RESULTS AND DISCUSSION

Contents of the Red mPGES-2. The purified red enzyme was treated with sodium citrate/HCl to make a solution acidic (pH 4.6) and then extracted with 2-butanone. The red solution was analyzed with a VG ZAB high-resolution double-focusing instrument. A positive electron spray spectrum exhibited a 616.0 nm peak, which corresponds to the molecular weight of ferroprotoporphyrin IX. A positive electron spray spectrum of pure hematin (heme) from Sigma also showed the same 616.2 nm peak, suggesting the red enzyme contains heme.

An EPR spectrum was measured at liquid helium temperature (4 K). It showed a typical Fe^{3+} EPR spectrum,

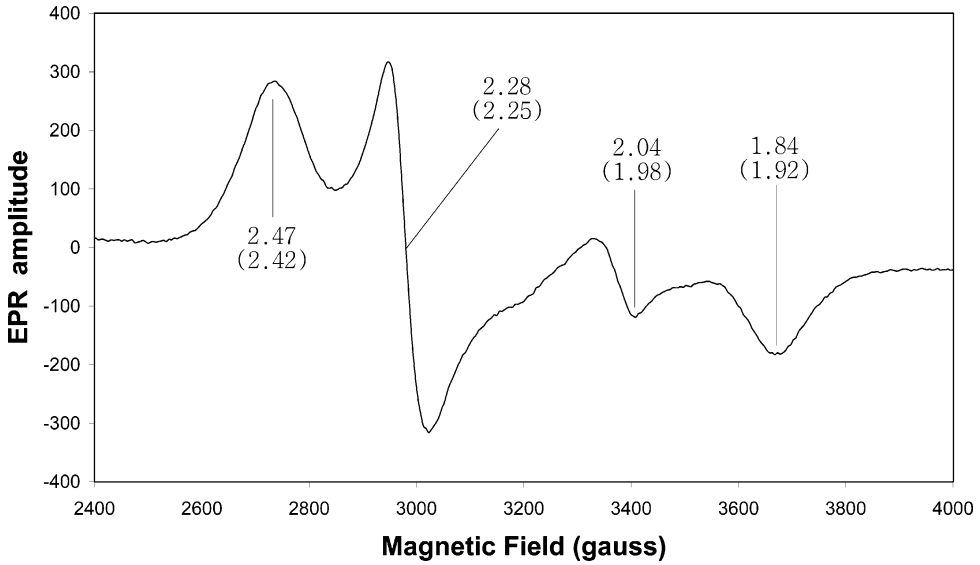

FIGURE 1: EPR spectrum of red mPGES-2h. Shown is the EPR spectrum in the low-spin heme region of the resting mPGES-2h. The *g* factors of mPGES-2h and TXAS (in parentheses) are given.

indicating that the red enzyme contains Fe^{3+} (Figure 1). Thromboxane A_2 synthase (TXAS) is a heme-containing protein, and one of the Cys residues coordinates to the heme iron (*29*, *30*), which has been characterized by EPR spectroscopy. The EPR spectra of red mPGES-2 and TXAS are quite similar. For example, the **g** tensor values of heme are 2.47, 2.28, and 1.84 for the red mPGES-2 and 2.42, 2.25, and 1.92 for TXAS (*31*). On the basis of the mass and EPR spectra, we conclude that the red colored enzyme contains Fe^{3+}-heme.

mPGES-2 Expression Stimulates Heme Biosynthesis. When the recombinant clone *E. coli* HB101 containing the mPGES-2 gene was grown in LB medium and overexpressed via addition of IPTG, a reddish enzyme (partially heme bound mPGES-2) was purified. When the recombinant clone *E. coli* was grown in LB medium containing $Fe(NO_3)_3$ and ALA, which are precursors of heme biosynthesis, the red enzyme (heme-bound mPGES-2) was obtained. On the other hand, the enzyme purified from the same recombinant clone *E. coli* grown in minimal medium was colorless. As described below, hPGDS is functionally similar to mPGES-2 and contains a GSH in the active site, and the active site geometry is quite similar to that of mPGES-2 (*32*). The overexpression experiment was carried out with the recombinant clone *E. coli* HB101 containing the hPGDS gene. However, no heme overproduction was observed. These experiments suggest that heme is overproduced along with mPGES-2 overexpression because the active site of mPGES-2 has a strong heme affinity and significantly decreases the concentration of free heme in cells. Therefore, mPGES-2 is not only an enzyme for catalyzing formation of PGE_2 from PGH_2 but also a free heme scavenger in cells. As discussed below, the heme-bound mPGES-2 catalyzes a completely different reaction.

Crystal Structure of mPGES-2h. Previously, the reddish enzyme purified from the same recombinant clone *E. coli* grown in LB medium was crystallized with an inhibitor indomethacin (IMN), and its crystal structure was determined at 2.6 Å resolution (*24*). However, the crystal structure does not exhibit significant electron density for bound heme, and we concluded that heme might bind to the disordered His tag (*24*). We have crystallized the red enzyme without IMN and determined the crystal structure, to elucidate the heme binding site.

Table 1: Experimental Details and Refinement Parameters of Crystal Structure Analyses[a]

Experimental Details	
resolution (Å)	10.0−2.8
no. of crystals	1
no. of reflections measured	83985
no. of unique reflections	35201
% complete	90.6 (84.3)[b]
R_{merge}[c]	0.074 (0.232)[b]
$I/\sigma(I)$	6.8 (4.8)[b]
Refinement Parameters	
no. of residues	1096
no. of GSH molecules	4
no. of heme molecules	4
no. of chlorine ions	4
no. of waters	167
R_{cryst}[d]	0.242
R_{free}	0.269
rmsd from ideal values	
bonds (Å)	0.007
angles (deg)	1.15
torsion angles (deg)	26.2
Luzzati coordinare error (Å)	0.039
Ramachandran plot (%)	
residues in most favored regions	88.5
residues in additional allowed regions	10.9

[a] Space group *C*2; cell dimensions, $a = 127.00$ Å, $b = 122.49$ Å, $c = 110.20$ Å, $\beta = 111.0°$; M_r of subunit, 37 000; no. of subunits in the unit cell, 16; $V_M = 2.77$ Å^3; percentage of solvent content, 55% (v/v). [b] Outer shell, 2.8−2.9 Å resolution. [c] $R_{merge} = \sum_h\sum_i|I_{hi} - \langle I_h\rangle|/\sum_h\sum_i|I_{hi}|$. [d] $R_{cryst} = \sum||F_o| - |F_c||/\sum|F_o|$.

The structure was determined at 2.8 Å resolution. The N-terminal section (His tag and residues 88−99) of each subunit was not determined due to disorder. The crystallographic refinement parameters (Table 1), final $2F_o - F_c$ and $F_o - F_c$ maps, and conformational analysis by PROCHECK (*33*) indicate that the structure of mPGES-2h has been determined with acceptable statistics. A crystallographic asymmetric unit contains four subunits related by a noncrystallographic 222 symmetry. The two subunits interact strongly and form a dimer, while the dimer−dimer

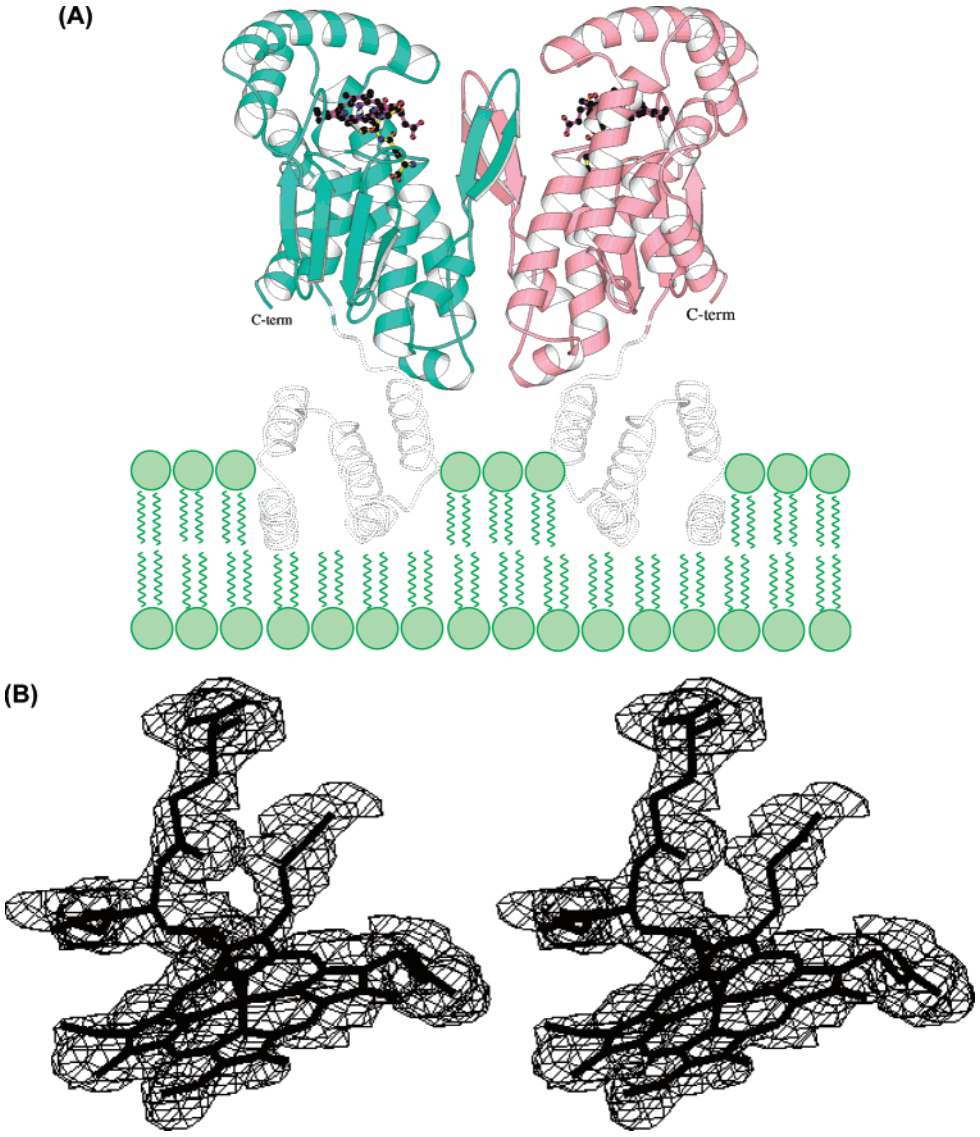

FIGURE 2: (A) Dimeric mPGES-2h sits on the lipid bilayer. Two subunits are shown in aquamarine and light pink. The bound GSH−heme complexes are illustrated in ball-and-stick mode. Parts of the truncated N-terminal section (residues 1−89) are apparently inserted into the lipid bilayer. (B) $F_o - F_c$ map showing the residual electron density peak of the bound GSH−heme complex. The final model of the GSH−heme complex is superimposed, and the contour is drawn at the 2.0σ level.

interaction is apparently weak (Figure 2A). The four independent subunits are identical at a resolution of 2.8 Å (rmsd ≤ 0.06 Å). Each subunit contains a GSH−heme complex in the active site, so the red-colored enzyme is a GSH−heme complex-bound mPGES-2 (in this article, we use mPGES-2[GSH−heme] or mPGES-2h as an abbreviation) (Figure 2). The structure of mPGES-2[GSH−heme] is isomorphous to that found in mPGES-2[IMN] (*24*). The rmsd between the two mPGES-2 structures is 0.56 Å, indicating that the three-dimensional structures of mPGES-2 in mPGES-2[GSH−heme] and mPGES-2[IMN] are the same within experimental error. Despite large differences in the molecular shapes and masses between IMN and the GSH−heme complex, binding of IMN or the GSH−heme complex does not alter the structure of mPGES-2, indicating that the active site of mPGES-2 is relatively large.

The porphyrin ring of heme and the indole ring of IMN are located at the same place. A GSH binds between the protein and the bound heme and forms six H-bonds with mPGES-2. Since the SH group of GSH is involved in a unique S−H···S−H···S−H H-bond chain formed by C113, C110, and GSH, it might be polarized to S^- and readily form a S−Fe coordinate bond with the bound heme (Figure 3). There is no H-bond between the heme and mPGES-2, indicating that the heme is mainly attached by hydrophobic interaction. The sixth coordination site is apparently occupied by an unknown small molecule (water or acetate), and thus, there is a large open space between the heme and the protein, where a PGH_2 might be able to bind.

The Fold of mPGES-2 Is Similar to That of hPGDS. The crystal structure of the functionally similar hPGDS has been determined (*28*, *32*, *34*). hPGDS belongs to the GSTase family, and the fold of hPGDS is quite similar to those of known GSTases [α class (*35*), μ class (*36*), π class (*37*), and σ class (*38*)]. Interestingly, the fold of mPGES-2 is similar to those of hPGDS and GSTases. By using SARF2 (*39*), the structure of mPGES-2 was compared with that of hPGDS (PDB entry 1PD2). One hundred fifty-nine C_A atoms (79%) of hPGDS can be superimposed on the corresponding C_A positions of mPGES-2 with rmsd's of 2.34 Å. Indeed, as

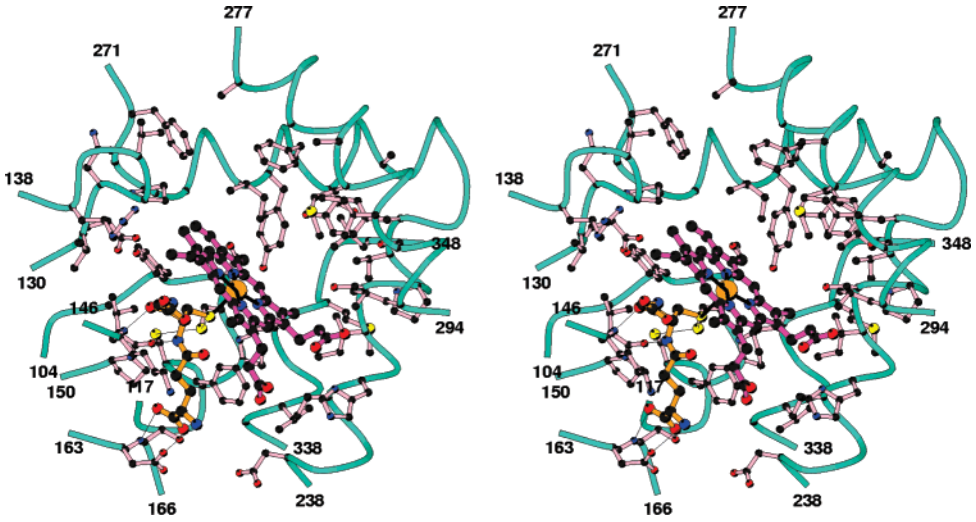

FIGURE 3: GSH−heme complex binding site showing interactions between the bound GSH−heme complex and mPGES-2. Thin lines indicate important H-bonds.

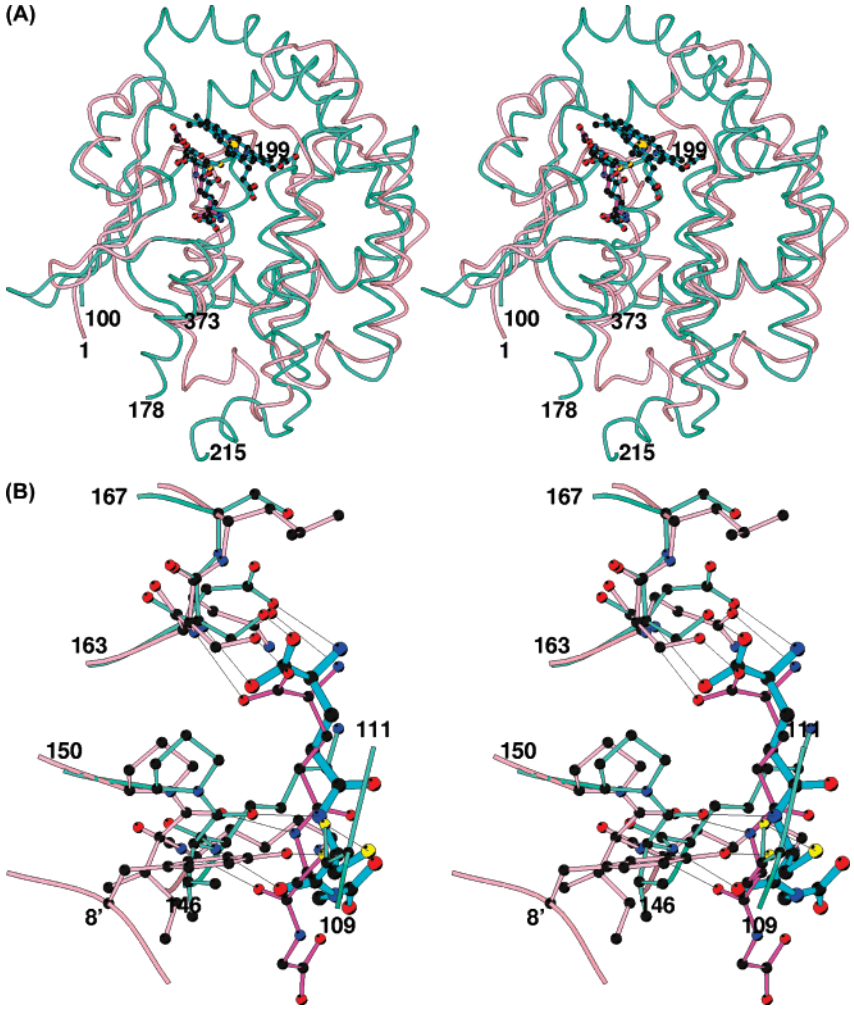

FIGURE 4: (A) Superimposed view of the structures of mPGES-2h (aquamarine, residues 100−373) and hPGDS (light pink, residues 1−199). Residues 179−214 of mPGES-2h have been omitted for the sake of clarity. The bound GSH−heme complex (cyan) and GSH (magenta) are shown. (B) Magnified view of the superimposed diagram showing the relative positions of GSH in mPGES-2h and GSH in hPGDS. The conserved H-bonds seen in the GST family are shown as thin lines. Those of GSH···mPGES-2h are Glu O_1···O_G S165, Glu O_2···N S165, Glu N···O_{D1} D164, Cys N···O V148, Cys O···N V148, and Cys S_G···S_G C110.

shown in Figure 4A, the main chain of mPGES-2 can be nearly superimposed on that of hPGDS except for the central domain region (residues 178−215), the helix−loop−helix region (residues 249−301), and the C-terminal. Interestingly, the bound GSH molecules are located at the same position in a superimposed hPGDS−mPGES-2 structure (Figure 4B). However, the percentage of identical residues in the superimposable section is relatively small (12%).

Rife et al. (*40*) have reported that the GSTase family has a consensus sequence, VP-L···(E/D)S--I. A similar sequence is seen in mPGES-2 (^{148}VP-L···^{164}DS--I). Furthermore, the bound GSH forms H-bonds with these conserved residues. For example, the amide and carbonyl groups of the Cys residue in GSH form a pair of H-bonds with those of V148, the carboxyl group of the Glu residue in GSH forms a pair of H-bonds with the amide (N) and hydroxyl (O_G) of S165, and the N-terminal amino group of GSH interacts with the carboxyl group of D164. These H-bonds and the salt linkage have been observed in the structures of the GSTase family, including hPGDS (*32*) (Figure 4B). On the basis of the similarities of the polypeptide fold, sequence, and GSH binding scheme, mPGES-2 should belong to the GSTase family, and therefore, GSH binds to the active site of mPGES-2 under physiological conditions.

Watanabe et al. (*23*) have reported that mPGES-2 is a GSH-independent enzyme, and DTT (0.5 mM) is the best cofactor examined thus far. Although the catalytic rate is increased 2−4-fold in the presence of GSH, it is significantly lower than that in the presence of DTT (*23*). The catalytic activity reaches a maximum at 0.1 mM GSH and is decreased with an increase in the GSH concentration. Their observations are inconsistent with the crystal structure and the sequence analysis described above. In the proposed catalytic mechanisms of hPGDS (*32*) and mPGES-2 (*24*), one RSH (bound GSH or Cys) is involved in the endoperoxide breakage and another RSH participates in the abstraction of hydrogen attached to C9 or C11 of PGH_2. Perhaps the second RSH might be responsible for the increased activity by DTT.

Heme Binding Analyzed by Tryptophan Fluorescence Spectra. Trp residues in proteins emit fluorescence (∼340 nm) with an excitation wavelength of 280 nm. Hematin (heme) does not fluoresce but absorbs radiation between 300 and 450 nm. Since a heme near Trp residues (i.e., a bound heme) absorbs fluorescence emitted from Trp residues, it is possible to examine the heme binding scheme, including the heme dissociation constant (K_d).

As shown in Figure 5A, heme titration quenches the fluorescence intensity but does not shift the spectrum, indicating that no major structural change occurred upon heme binding. The individual fluorescence spectra (f_i) titrated with various amounts of heme were examined whether the individual f_i values were represented by the heme-free spectrum (f_o) with the individual scale factors (S_i); i.e., $f_i = S_i f_o$. The individual scale factors were obtained by a least-squares method ($S_i = \sum f_o f_i / \sum f_o^2$). The agreement factor ($\sum|f_i - S_i f_o|/\sum f_i$) between the observed ($f_i$) and calculated fluorescence spectra ($S_i f_o$) was less than 0.012, indicating that the individual spectra are indeed represented by the scaled heme-free spectrum. The $1 - S_i$ value that expresses the fractional reduction of the fluorescence intensity of the heme-free enzyme also represents the fractional saturation of ligand. A plot of $1 - S_i$ versus heme concentration shows a hyperbolic curve (Figure 5B), and the double-reciprocal plot shows good linearity with an intercept near 1 of the *y*-axis (Figure 5C). The fractional saturation (Y) and dissociation constant (K_d) are defined by the relationships $Y = [PL]/([P] + [PL])$ and $K_d = ([P][L])/[PL]$, respectively, where [P], [PL], and [L] are the concentrations of heme-free protein, heme-bound protein, and heme, respectively. Expressing the fractional saturation as $Y = [L]/(K_d + [L])$ allows the dissociation constant (K_d) to be calculated from the ligand concentration at 50% saturation (Figure 5B) or the slope of the double-reciprocal plot (Figure 5C). The obtained dissociation constant (K_d) is 0.54 μM.

In the heme titration experiment, the heme or GSH−heme association was actually assessed, but not the heme dissociation. The heme dissociation constant might be smaller than the calculated dissociation constant since the bound heme is needed to break the S−Fe coordination bond to dissociate. Because mPGES-2 exists as a dimer, a bound heme on one of subunits could absorb fluorescence from both subunits. Therefore, the fluorescence quenching by the heme binding may not simply express the fractional saturation of ligand, and thus, the dissociation constant obtained in this study is an apparent dissociation constant.

In general, hemes in heme proteins are buried in a hydrophobic pocket so that the heme does not dissociate from the protein under physiological conditions and the dissociation constant is relatively small ($<10^{-9}$ M). In the crystal structure of mPGES-2[GSH−heme], one side of the heme attaches to mPGES-2 and the bound GSH with hydrophobic interactions, but the other side is exposed to solvent. Therefore, the bound heme in mPGES-2 is dissociable; i.e., the dissociation constant is relatively large ($>10^{-7}$ M) in comparison with those of typical heme proteins such as hemoglobin [$K_d = 10^{-14}$ M (*41*)].

Catalytic Activity of mPGES-2h. A preliminary assay had indicated that mPGES-2h did not catalyze formation of PGE_2 from PGH_2. As discussed below, a sequence analysis suggested that mPGES-2h might catalyze formation of TxA_2 or 12(*S*)-hydroxy-5(*Z*),8(*E*),10(*E*)-heptadecatrienoic acid (HHT) from PGH_2. Therefore, we carefully analyzed the reaction mixtures by HPLC and found that PGH_2 was broken down into HHT and malondialdehyde (MDA) by mPGES-2h. The reactions were carried out at 4 °C, to minimize the nonenzymatic degradation of PGH_2. The kinetic parameters of formation of HHT from PGH_2 by mPGES-2h at 4 °C were determined: $K_M = 56$ μM and $k_{cat} = 2.7$ s^{-1} (Figure 6). The k_{cat} at 37 °C was estimated from the k_{cat} at 4 °C using the transition state theory equation $k_{cat} = (k_B T/h)e^{-\Delta G^*/RT}$, where k_B, h, and R are the Boltmann constant, Planck's constant, and gas constant, respectively. In the calculation, the free energy at the transition state, ΔG^*, was assumed to be constant between 277 and 310 K. The estimated k_{cat} at 37 °C is 63 s^{-1}, and the catalytic efficiency (k_{cat}/K_M) at 37 °C is 1.1×10^6 M^{-1} s^{-1}, suggesting that mPGES-2h has a significant catalytic activity for PGH_2 degradation.

Since PGH_2 readily breaks down nonenzymatically (*42*), we carried out an assay with the enzyme boiled at 95 °C, and no HHT production was detected by HPLC analyses. The catalytic activities of heme and the GSH−heme complex were also examined at the same concentration of mPGES-2h (0.135 μM), but no HHT production was detected by HPLC analyses, confirming that PGH_2 is degraded to HHT and MDA by mPGES-2h. Formation of prostanoids from PGH_2 by mPGES-2h was also examined by HPLC. The reaction mixtures did not show any significant peaks corresponding to PGE_2, PGD_2, or $PGF_{2\alpha}$, indicating that mPGES-2h does not catalyze formation of PGE_2 from PGH_2 as heme-free mPGES-2 does.

The kinetic parameters of formation of PGE_2 from PGH_2 by mPGES-2 have been reported to be K_M 24 μM and k_{cat}

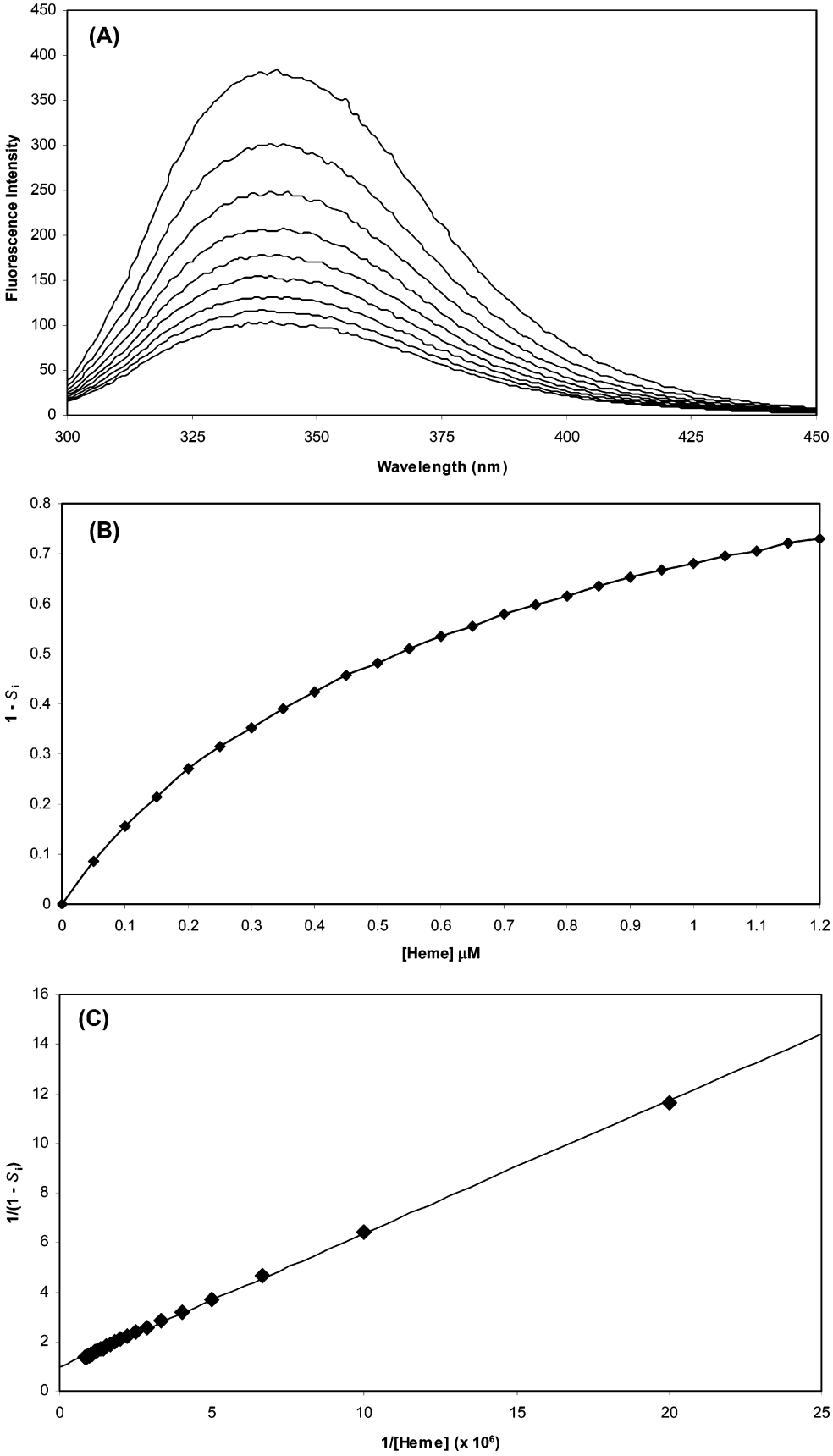

FIGURE 5: (A) Quenching of Trp fluorescence by heme. The heme concentrations are 0.0, 0.15, 0.30, 0.45, 0.60, 0.75, 0.90, 1.05, and 1.20 μM from top to bottom. (B) Plot showing a relation between the heme concentration and fluorescence quenching by heme titration. The *x*- and *y*-axes are heme concentration (micromolar) and $1 - S_i$, respectively, where S_i is a relative scale factor of the *i*th fluorescence spectrum obtained by a least-squares minimization ($S_i = \sum f_o f_i / \sum f_o^2$). (C) Double-reciprocal plot of panel B. The slope and intercept of the extrapolated line are 0.54×10^{-6} and 0.98, respectively.

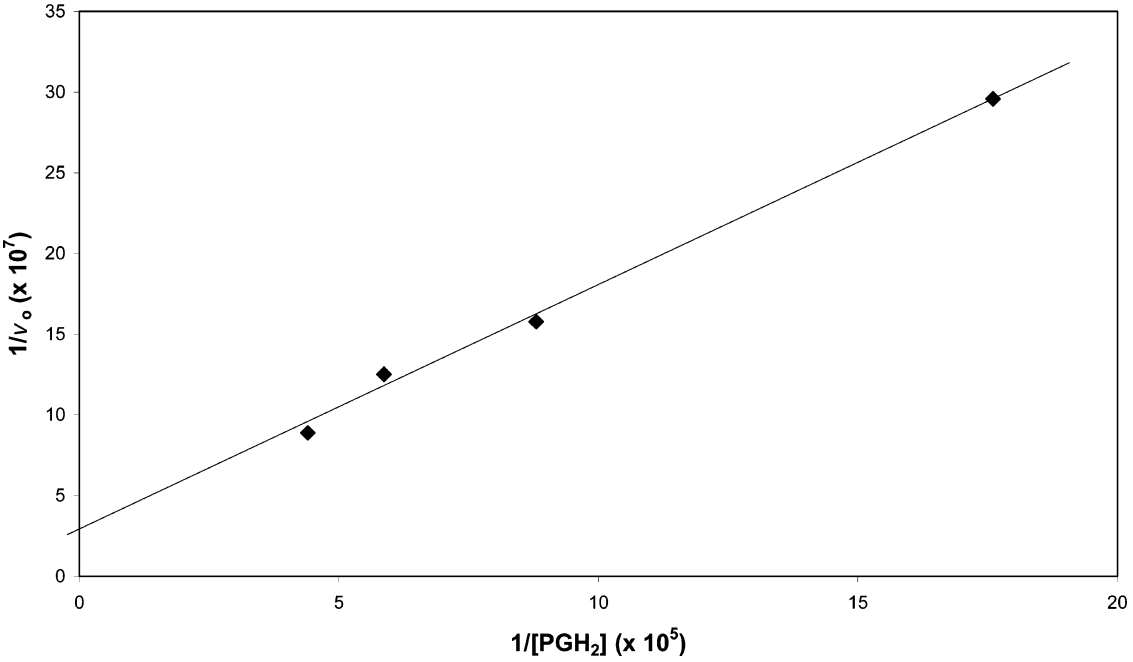

FIGURE 6: Double-reciprocal plot of formation of HHT from PGH_2. The *x*- and *y*-axes are reciprocals of the PGH_2 concentration and initial velocity (v_o) of the reaction, respectively. The protein concentration and molecular weight (M_r) are 5.0 mg/L and 37 000, respectively, and the slope and intercept of the extrapolated line are 1.53×10^2 and 2.70×10^6, respectively. On the basis of these values, the V_{max} of 5 μg/mL protein, K_M, and k_{cat} are calculated to 3.70×10^{-7} mol/s, 56 μM, and 2.7 s^{-1}, respectively.

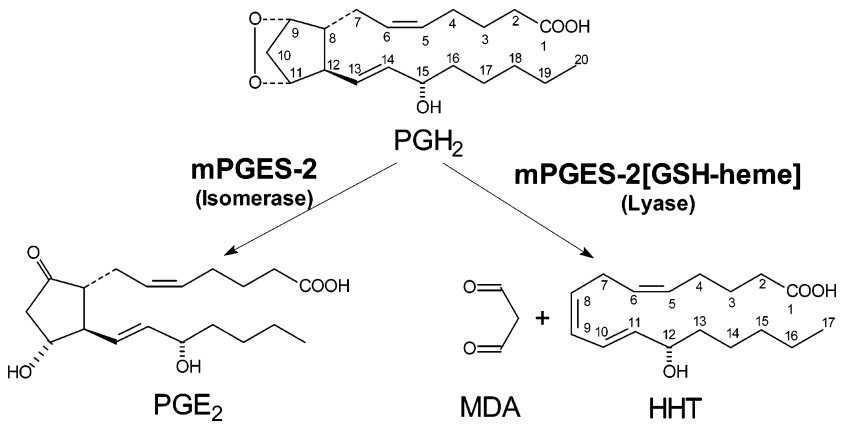

FIGURE 7: Two different reactions catalyzed by mPGES-2 and mPGES-2h.

0.43 s^{-1} for the rat heart enzyme at 24 °C (*22*) and 28 μM (K_M) and 1.82 s^{-1} (k_{cat}) for the recombinant enzyme at 24 °C (*23*). The estimated k_{cat} values at 37 °C of the rat heart and recombinant enzymes are 1.6 and 6.4 s^{-1}, respectively. The catalytic efficiency (k_{cat}/K_M) at 37 °C of the recombinant enzyme is 2.3×10^5 M^{-1} s^{-1}, suggesting that the heme-free and heme-bound enzymes catalyze formation of PGE_2 and HHT, respectively, at similar rates.

The free heme concentrations of various tissues have not been well defined. The newly synthesized mPGES-2 becomes mPGES-2h if the heme concentration is relatively high. COX and TXAS are involved in the PGH_2 metabolism and are heme-containing enzymes, suggesting that heme would be available to some of the newly synthesized mPGES-2 to become mPGES-2h in cells, where PGH_2 is metabolized. Therefore, it is possible that both GSH−heme complex-free and -bound enzymes are present in the same tissues. The two major sites of heme biosynthesis are erythroid cells, which synthesize ~85% of the body's heme groups, and the liver, which synthesizes most of the remainder (*43*). The mRNA of mPGES-2 has been detected in various human tissues, including liver, by dot blot analysis (*23*). Therefore, mPGES-2 in heme-rich liver is most likely to become the form of mPGES-2h and might be involved in degradation reactions similar to that of cytochrome P450 (*44*).

The GSH−Heme Complex-Bound C110S Mutated Enzyme Has PGH_2 Degradation Activity. The C110S mutation abolishes PGES activity, but the C113S mutated enzyme retains catalytic activity (*25*). The crystal structure of mPGES-2h suggests that neither the C110S mutation nor the C113S mutation disrupts the characteristic H-bond chain (SH···SH···SH) seen through C113···C110···GSH. The C110S mutated enzyme-purified *E. coli* HB101 grown in LB medium containing ALA and $Fe(NO_3)_3$ had a red color, indicating that the GSH−heme complex binds to the active site as seen in the mPGES-2h structure. This red enzyme has a similar PGH_2 degradation activity as observed in

mPGES-2h. Therefore, binding of the GSH−heme complex to the active site generates a new catalytic activity to a mutated inactive enzyme.

mPGES-2h and TXAS Might Have Similar Structures and Catalytic Mechanisms of Formation of HHT from PGH_2. HHT has been shown to be produced from PGH_2 by TXAS, COX-1, and COX-2. TXAS converts PGH_2 into TxA_2, HHT, and MDA in a 1:1:1 ratio (*45*). COX-1 and COX-2 convert 88 and 78% of arachidonic acid, respectively, to HHT and MDA through PGH_2 in the presence of GSH (1 mM) (*46*). Since mPGES-2h, TXAS, COX-1, and COX-2 are heme-containing proteins and the heme is apparently involved in the catalytic reactions similar to that of cytochrome P450 (*44*), formation of HHT from PGH_2 might be due to a common catalytic mechanism.

TXAS is a heme-containing but GSH-lacking protein. EPR studies indicate that the iron in TXAS is Fe^{3+}, and a thiolate coordinates at the heme iron (*29*, *30*). As shown in Figure 1, an EPR spectrum of mPGES-2h is quite similar to that of TXAS. The amino acid sequences of mPGES-2 and TXAS were aligned by using CLUSTAL W (version 1.81), and these two enzymes are relatively well aligned [i.e., 47.8% of amino acid residues are either identical (14.6%), conservatively substituted (18.6%), or semiconservatively substituted (14.6%)]. The EPR studies and the sequence alignment suggest that their peptide folds and the active site geometries might be similar. According to the mechanism proposed by Hecker and Ullrich (*30*), TXAS catalyzes formation of TxA_2, HHT, and MDA from PGH_2 at the same catalytic site, and the endoperoxide (−O−O−) of PGH_2 is opened by interacting with the heme iron (Fe^{3+}). A simple modeling of mPGES-2[GSH−heme + PGH_2] suggests that PGH_2 can bind on the bound heme, placing the endoperoxide moiety near the heme iron (Fe^{3+}). In this geometry, a catalytic reaction similar to the TXAS reaction might occur.

mPGES-2 Is the First Example that Catalyzes Two Different Reactions. The International Union of Biochemistry and Molecular Biology (IUBMB) has determined that every enzyme is classified into one of six classes [(1) oxidoreductase, (2) transferase, (3) hydrolase, (4) lyase, (5) isomerase, and (6) ligase] according to the nature of the chemical reactions they catalyze. For example, PGES belongs to the isomerase class (EC class 5).

TXAS ($PGH_2 \rightarrow TxA_2$ or HHT + MDA) and COX (arachidonic acid → PGH_2 or HHT + MDA) apparently catalyze two different reactions at the same active site; i.e., the activated PGH_2 (transition state molecule) in the active site is converted to either HHT and MDA or the product (*43*, *44*). On the other hand, the catalytic cavity of mPGES-2 is modified by binding of a GSH−heme complex, and the GSH−heme complex-bound enzyme catalyzes degradation of PGH_2 to HHT and MDA but not isomerization, while the GSH−heme complex-free enzyme catalyzes isomerization of PGH_2 to PGE_2 but not degradation. Therefore, the nature of the dual functions of mPGES-2 is not the same as those of TXAS and COX. As summarized in Figure 7, GSH−heme complex-free mPGES-2 belongs to the isomerase class (EC class 5) while GSH−heme complex-bound mPGES-2 (mPGES-2h) belongs to the lyase class (EC class 4), which catalyzes an elimination that creates an unsaturated bond. Therefore, mPGES-2 cannot simply be classified into one of the six classes set by the IUBMB. As far as we know, mPGES-2 is the first example of an enzyme whose catalytic function is altered by addition of cofactors.

ACKNOWLEDGMENT

We express our thanks to Professor Kikuko Watanabe for providing us plasmids encoded mPGES-2 and C110S mutated mPGES-2, Professor Andrew Borovik for allowing us to use his EPR equipment, and Professor Richard H. Himes for a critical reading of the manuscript and very valuable comments.

REFERENCES

1. Smith, W. L., Marnett, L. J., and DeWitt, D. L. (1991) Prostaglandin and thromboxane biosynthesis, *Pharmacol. Ther. 49*, 153−179.
2. Vander, A. J. (1968) Direct effects of prostaglandin on renal function and rennin release in anesthetized dog, *Am. J. Physiol. 214*, 218−221.
3. Milton, A. S., and Wendlandt, S. (1971) Effects on body temperature of prostaglandins of the A, E, and F series on injection into the third ventricle of unanaesthetized cats and rabbits, *J. Physiol. 218*, 325−336.
4. Matsumura, H., Goh, Y., Ueno, R., Sakai, T., and Hayaishi, O. (1988) Awaking effects of PGE_2 microinjected into the preoptic area of rats, *Brain Res. 444*, 265−272.
5. Hayaishi, O. (1991) Molecular mechanisms of sleep-wake regulation: Roles of prostaglandins D_2 and E_2, *FASEB J. 5*, 2575−2581.
6. Lawrence, T., Willoughby, D. A., and Gilroy, D. W. (2002) Anti-inflammatory lipid mediators and insights into the resolution of inflammation, *Nat. Rev. Immunol. 2*, 787−795.
7. Williams, T. J., and Peck, M. J. (1977) Role of prostaglandin-mediated vasodilatation in inflammation, *Nature 270*, 530−532.
8. Raud, J., Dahlén, S.-E., Sydbom, A., Lindbom, L., and Hedqvist, P. (1988) Enhancement of acute allergic inflammation by indomethacin is reversed by prostaglandin E_2: Apparent correlation with *in vivo* modulation of mediator release, *Proc. Natl. Acad. Sci. U.S.A. 85*, 2315−2319.
9. Dinarello, C. A., Bernheim, H. A., Duff, G. W., Le, H. V., Nagabhushan, T. L., Hamilton, N. C., and Coceani, F. (1984) Mechanisms of fever induced by recombinant human interferon, *J. Clin. Invest. 74*, 906−913.
10. Ballou, L. R. (2002) in *Eicosanoids and Other Bioactive Lipids in Cancer, Inflammation, and Radiation Injury* (Honn, K. V., Marnett, L. J., Nigam, S., and Serhan, C. N., Eds.) Vol. 5, pp 585−591, Kluwer/Plenum, New York.
11. Thoren, S., and Jakobsson, P. J. (2000) Coordinate up- and down-regulation of glutathione-dependent prostaglandin E synthase and cyclooxygenase-2 in A549 cells. Inhibition by NS-398 and leukotriene C4, *Eur. J. Biochem. 267*, 6428−6434.
12. Greco, A., Ajmone-Cat, M. A., Nicolini, A., Sciulli, M. G., and Minghetti, L. (2003) Paracetamol effectively reduces prostaglandin E_2 synthesis in brain macrophages by inhibiting enzymatic activity of cyclooxygenase but not phospholipase and prostaglandin E synthase, *J. Neurosci. Res. 71*, 844−852.
13. Ogorochi, T., Ujihara, M., and Narumiya, S. (1987) Purification and properties of prostaglandin H-E isomerase from the cytosol of human brain: Identification as anionic forms of glutathione S-transferase, *J. Neurochem. 48*, 900−909.
14. Meyer, D. J., Muimo, R., Thomas, M., Coates, D., and Isaac, R. E. (1996) Purification and characterization of prostaglandin-H E-isomerase, a sigma-class glutathione S-transferase, from *Ascaridia galli*, *Biochem. J. 313*, 223−227.
15. Tanioka, T., Nakatani, Y., Semmyo, N., Murakami, M., and Kudo, I. (2000) Molecular identification of cytosolic prostaglandin E_2 synthase that is functionally coupled with cyclooxygenase-1 in immediate prostaglandin E_2 biosynthesis, *J. Biol. Chem. 275*, 32775−32782.
16. Ogino, N., Miyamoto, T., Yamamoto, S., and Hayaishi, O. (1977) Prostaglandin endoperoxide E isomerase from bovine vesicular gland microsomes, a glutathione-requiring enzyme, *J. Biol. Chem. 252*, 890−895.

17. Moonen, P., Buytenhek, M., and Nugteren, D. H. (1982) Purification of PGH-PGE isomerase from sheep vesicular glands, *Methods Enzymol. 86*, 84−91.
18. Tanaka, Y., Ward, S. L., and Smith, W. L. (1987) Immunochemical and kinetic evidence for two different prostaglandin H prostaglandin E isomerases in sheep vesicular gland microsomes, *J. Biol. Chem. 262*, 1374−1381.
19. Jakobsson, P. J., Thoren, S., Morgenstern, R., and Samelsson, B. (1999) Identification of human prostaglandin E synthase: A microsomal glutathione-dependent, inducible enzyme, constituting a potential novel drug target, *Proc. Natl. Acad. Sci. U.S.A. 96*, 7220−7225.
20. Thoren, S., Weinander, R., Saha, S., Jegerschold, C., Pettersson, P. L., Samuelsson, B., Hebert, H., Hamberg, M., Morgenstern, R., and Jakobsson, P. J. (2003) Human microsomal prostaglandin E synthase-1: Purification, functional characterization, and projection structure determination, *J. Biol. Chem. 278*, 22199−22209.
21. Watanabe, K., Kurihara, K., and Hayaishi, O. (1997) Two types of micosomal prostaglandin E synthase: Glutathione-dependent and -independent prostaglandin E synthases, *Biochem. Biophys. Res. Commun. 235*, 148−152.
22. Watanabe, K., Kurihara, K., and Suzuki, T. (1999) Purification and characterization of membrane-bound prostaglandin E synthase from bovine heart, *Biochim. Biophys. Acta 1439*, 406−414.
23. Tanikawa, N., Ohmiya, Y., Ohkubo, H., Hashimoto, K., Kangawa, K., Kojima, M., Ito, S., and Watanabe, K. (2002) Identification and characterization of a novel type of membrane-associated prostaglandin E synthase, *Biochem. Biophys. Res. Commun. 291*, 884−889.
24. Yamada, T., Komoto, J., Watanabe, K., Ohmiya, Y., and Takusagawa, F. (2005) Crystal structure and possible catalytic mechanism of microsomal prostaglandin E synthase type 2 (mPGES-2), *J. Mol. Biol. 348*, 1163−1176.
25. Watanabe, K., Ohkubo, H., Niwa, H., Tanikawa, N., Koda, N., Ito, S., and Ohmiya, Y. (2003) Essential 110Cys in active site of membrane-associated prostaglandin E synthase-2, *Biochem. Biophys. Res. Commun. 306*, 577−581.
26. Otwinowski, Z., and Minor, W. (1997) Processing of X-ray diffraction data collected in oscillation mode, *Methods Enzymol. 276*, 307−326.
27. Brünger, A. T., Adams, P. D., Clore, G. M., DeLano, W. L., Gros, P., Grosse-Kunstleve, R. W., Jiang, J. S., Kuszewski, J., Nilges, M., Pannu, N. S., Read, R. J., Rice, L. M., Simonson, T., and Warren, G. L. (1998) Crystallography & NMR system: A new software suite for macromolecular structure determination, *Acta Crystallogr. D54*, 905−921.
28. Inoue, T., Irikura, D., Okazaki, N., Kinugasa, S., Matsumura, H., Uodome, N., Yamamoto, M., Kumasaka, T., Miyano, M., Kai, Y., and Urade, Y. (2003) Mechanism of metal activation of human hematopoietic prostaglandin D synthase, *Nat. Struct. Biol. 10*, 291−296.
29. Haurand, M., and Ullrich, V. (1985) Isolation and characterization of thromboxane synthase from human platelets as a cytochrome P-450 enzyme, *J. Biol. Chem. 260*, 15059−15067.
30. Hecker, M., and Ullrich, V. (1989) On the mechanism of prostacyclin and thromboxane A_2 biosynthesis, *J. Biol. Chem. 264*, 141−150.
31. Hsu, P. Y., Tsai, A. L., Kulmacz, R. J., and Wang, L. H. (1999) Expression, purification, and spectroscopic characterization of human thromboxane synthase, *J. Biol. Chem. 274*, 762−769.
32. Kanaoka, Y., Ago, H., Inagaki, E., Nanayama, T., Miyano, M., Kikuno, R., Fujii, Y., Eguchi, N., Toh, H., Urade, Y., and Hayaishi, O. (1997) Cloning and crystal structure of hematopoietic prostaglandin D synthase, *Cell 90*, 1085−1095.
33. Laskowski, R. A., MacArthur, M. W., Moss, D. S., and Thornton, J. M. (1993) PROCHECK: A program to check the stereochemical quality of protein structures, *J. Appl. Crystallogr. 26*, 283−291.
34. Inoue, T., Okano, Y., Kado, Y., Aritake, K., Irikura, D., Uodome, N., Okazaki, N., Kinugasa, S., Shishitani, H., Matsumura, H., Kai, Y., and Urade, Y. (2004) First determination of the inhibitor complex structure of human hematopoietic prostaglandin D synthase, *J. Biochem. 135*, 279−283.
35. Sinning, I., Kleywegt, G. J., Cowan, S. W., Reinemer, P., Dirr, H. W., Huber, R., Gilliland, G. L., Armstrong, R. N., Ji, X., Board, P. G., et al. (1993) Structure determination and refinement of human α class glutathione transferase A1-1, and a comparison with the μ and π class enzymes, *J. Mol. Biol. 232*, 192−212.
36. Raghunathan, S., Chandross, R. J., Kretsinger, R. H., Allison, T. J., Penington, C. J., and Rule, G. S. (1994) Crystal structure of human class μ glutathione transferase GSTM2-2. Effects of lattice packing on conformational heterogeneity, *J. Mol. Biol. 238*, 815−832.
37. Reinemer, P., Dirr, H. W., Ladenstein, R., Schaffer, J., Gallay, O., and Huber, R. (1991) The three-dimensional structure of class π glutathione *S*-transferase in complex with glutathione sulfonate at 2.3 Å resolution, *EMBO J. 10*, 1997−2005.
38. Ji, X., von Rosenvinge, E. C., Johnson, W. W., Tomarev, S. I., Piatigorsky, J., Armstrong, R. N., and Gilliland, G. L. (1995) Three-dimensional structure, catalytic properties, and evolution of a σ class glutathione transferase from squid, a progenitor of the lens *S*-crystallins of cephalopods, *Biochemistry 34*, 5317−5328.
39. Alexandrov, N. N. (1996) SARFing the PDB, *Protein Eng. 9*, 727−732.
40. Rife, C. L., Parsons, J. F., Xiao, G., Gilliland, G. L., and Armstrong, R. N. (2003) Conserved structural elements in glutathione transferase homologues encoded in the genome of *Escherichia coli*, *Proteins 53*, 777−782.
41. Hargrove, M. S., Barrick, D., and Olson, J. S. (1996) The association rate constant for heme binding to globin is independent of protein structure, *Biochemistry 35*, 11293−11299.
42. Andersen, N. H., and Hartzell, C. J. (1984) High-field ^{1}H NMR studies of prostaglandin H2 and its decomposition pathway, *Biochem. Biophys. Res. Commun. 120*, 512−519.
43. Voet, D., and Voet, J. G. (2004) *Biochemistry*, 3rd ed., Vol. 1, John Wiley & Sons, Inc., New York.
44. Plastaras, J. P., Guengerich, F. P., Nebert, D. W., and Marnett, L. J. (2000) Xenobiotic-metabolizing cytochromes P450 convert prostaglandin endoperoxide to hydroxyheptadecatrienoic acid and the mutagen, malondialdehyde, *J. Biol. Chem. 275*, 11784−11790.
45. Diczfalusy, U., Falardeau, P., and Hammarstrom, S. (1977) Conversion of prostaglandin endoperoxides to C17-hydroxy acids catalyzed by human platelet thromboxane synthase, *FEBS Lett. 84*, 271−274.
46. Capdevila, J. H., Jason, D., Morrow, J. D., Belosludtsev, Y. Y., Beauchamp, D. R., DuBois, R. N., and Falck, J. R. (1995) The catalytic outcomes of the constitutive and the mitogen inducible isoforms of prostaglandin H_2 synthase are markedly affected by glutathione and glutathione peroxidases, *Biochemistry 34*, 3325−3337.

BI700605M